https://doi.org/10.5194/egusphere-2026-2798
Preprint. Discussion started: 1 June 2026

Surface impacts of Sudden Stratospheric Warmings (SSWs): Comparison of 2018 and 2019 SSWs in SNAPSI experiments

Dong-Chan Hong[1], Seok-Woo Son[1], Blanca Ayarzagüena[2], Amy H. Butler[3], Chaim I. Garfinkel[4], Peter Hitchcock[5], Yu-Kyung Hyun[6], Jiankai Zhang[7]

[1]School of Earth and Environmental Sciences, Seoul National University, Seoul, 08826, South Korea
[2]Department of Earth Physics and Astrophysics, Facultad de CC. Físicas, Universidad Complutense Madrid, Madrid, 28040, Spain
[3]National Oceanic and Atmospheric Administration (NOAA) Chemical Sciences Laboratory, Boulder, CO, 80305, USA
[4]Fredy and Nadine Herrmann Institute of Earth Sciences, The Hebrew University of Jerusalem, Jerusalem, 9190401, Israel
[5]Department of Earth and Atmospheric Sciences, Cornell University, Ithaca, NY, 14853, USA
[6]Forecast Technology Division, Korea Meteorological Administration, Seoul, 07062, South Korea
[7]College of Atmospheric Sciences, Lanzhou University, Lanzhou, 730000, China

Correspondence to: Seok-Woo Son (seokwooson@snu.ac.kr)

Abstract. Stratospheric Sudden Warmings (SSWs) significantly affect surface climate in boreal winter. However, their impacts vary considerably from one event to another: more than one-third of SSWs are not followed by expected tropospheric anomalies. To isolate the forced responses to SSWs, this study analyzes model experiments from the Stratospheric Nudging And Predictable Surface Impacts (SNAPSI) project, where the stratospheric zonal-mean state is nudged using either observations or climatology. The differences between the two experiments are examined within a multi-model ensemble framework. Nudging experiments conducted for the 2018 SSW, which featured significant tropospheric responses, and the 2019 SSW, which showed none, reveal that both SSWs consistently drive a negative Northern Annular Mode over time. The forced tropospheric response is primarily driven by an increase in Arctic surface pressure resulting from poleward mass fluxes in the stratosphere and upper troposphere. The poleward mass fluxes are initially induced by the zonal wind nudging in the middle stratosphere and subsequently by the eddy heat and momentum fluxes in the stratosphere and upper troposphere. This result suggests that while SSWs intrinsically drive tropospheric anomalies, the internal variability in the troposphere strengthens or suppresses the forced anomalies from the stratosphere, which may determine the existence of expected tropospheric anomalies following SSWs.

1 Introduction

A Sudden Stratospheric Warming (SSW) is one of the most drastic events in the stratosphere, characterized by a rapid temperature increase (e.g., Scherhag, 1952; Baldwin et al., 2021). During the event, the stratospheric polar vortex is disrupted and polar stratospheric winds reverse from a climatological westerly state to a weak easterly state. This polar vortex weakening or breakdown exerts a significant influence on the troposphere (e.g., Baldwin et al., 2021). Following SSW onset, the Northern

https://doi.org/10.5194/egusphere-2026-2798
Preprint. Discussion started: 1 June 2026

Annular Mode (NAM), the dominant mode of extratropical variability in the Northern Hemisphere, typically exhibits a negative phase in the troposphere for about two months (e.g., Baldwin and Dunkerton, 2001). This leads to surface extremes, such as cold air outbreaks across Eurasia and anomalously warm temperatures near Greenland (e.g., Butler et al., 2017; Domeisen and Butler, 2020). Given these impacts, SSWs have been widely investigated as one of the primary sources of subseasonal-to-seasonal prediction (S2S; e.g., Meehl et al., 2021; Butler et al., 2026).

However, not all SSWs are followed by expected surface anomalies. Karpechko et al. (2017) reported that only approximately 60% of SSWs are accompanied by a persistent negative phase of NAM within the troposphere. Several factors have been proposed to explain why some SSWs exert a downward influence while others do not. These factors include the morphology of the polar vortex, wave propagation characteristics, and the anomalous strength of the polar vortex in the lower stratosphere (e.g., Kodera et al., 2016; Karpechko et al., 2017; Hitchcock et al., 2013). However, their relative roles are not well quantified. The importance of internal variability in the troposphere relative to the forced response also remains to be determined.

Nudging experiments have increasingly been employed to isolate the forced response of the tropospheric circulation to an SSW and to identify the key factors determining SSW downward influence. Using a climate model, Hitchcock and Simpson (2016) compared SSW and climatology nudging experiments to examine the equatorward shift of the tropospheric jet following an SSW. Knight et al. (2021) performed extratropical stratospheric nudging experiments for the February 2018 SSW, which was followed by cold air outbreaks in Europe, and the January 2019 SSW, which exhibited nearly no surface response, by using a seasonal prediction system. The forced responses to both SSW events exhibit surface easterly anomalies following the SSW onset. Similarly, Huang et al. (2022) conducted observation and climatology nudging experiments in the stratosphere using a regional model. They reported that the stratosphere is a critical factor in the development of cold air outbreaks in Europe following the February 2018 SSW. Dai et al. (2025) further investigated the impact of the February 2018 SSW on record-breaking rainfall in the Iberian Peninsula using data from the Stratospheric Nudging And Predictable Surface Impacts (SNAPSI; Hitchcock et al., 2022) project, and concluded that the 2018 SSW significantly increased the potential for extreme precipitation in Iberia. While these and other nudging studies not cited here have described the downward influence of SSW and underlying dynamical processes, the mechanisms through which SSWs affect the tropospheric circulation and surface climate still remain to be determined.

The present study extends previous studies by examining stratospheric nudging experiments from the SNAPSI project. By comparing two distinct SSW events in the SNAPSI project, i.e., downward-influencing February 2018 SSW and non-downward-influencing January 2019 SSW in the Northern Hemisphere, we investigate the impacts of SSWs on tropospheric anomalies. As in previous studies, the forced responses are isolated by comparing the nudging experiments with the observed and climatological stratospheres. The mechanisms underlying the forced responses to SSWs are explored with the mass flux diagnostics as in Hong and Son (2025).

https://doi.org/10.5194/egusphere-2026-2798
Preprint. Discussion started: 1 June 2026

2 Data and Methodology

2.1 SNAPSI datasets

The SNAPSI project aims to identify the influence of SSW on S2S prediction by employing stratospheric nudging (Hitchcock et al., 2022), as well as to investigate the role of the stratosphere in other processes, such as upward wave flux and weather extremes (Ayarzagüena et al., 2026; Seviour et al., in review). The project involves three experiments: FREE, in which nudging is not applied; NUDGED, in which the zonal-mean stratospheric zonal wind and temperature are nudged toward ERA5 reanalysis (hereafter referred to as observations; Hersbach et al., 2020); and CONTROL, in which that the zonal-mean state is nudged toward the observational climatology. To confine the nudging to the stratosphere, the nudging strength gradually increases from 90 hPa to 50 hPa, above which it is fully applied with a 6-hour nudging timescale (see Hitchcock et al., 2022 for details). Only the zonal-mean component in the stratosphere is controlled in both experiments, the asymmetric component, such as waves, evolves freely. All experiments are initialized at two different lead times with two distinct objectives: a two-week lead initialization to assess SSW predictability, and a near-onset initialization to examine the subsequent downward influence, which is the primary focus of the present study.

Three SSW events across both hemispheres are considered in the SNAPSI project. They are two major SSWs in the Northern Hemisphere, occurring on 12 February 2018 and 2 January 2019, and one minor SSW in the Southern Hemisphere, which occurred on 18 September 2019. To investigate the surface response to the Northern Hemisphere SSW, the February 2018 SSW (SSW2018) and the January 2019 SSW (SSW2019) are examined in this study. SSW2018 is characterized by a visible negative NAM in the troposphere and cold air outbreaks in Europe, and classified as a downward-influencing SSW based on Karpechko et al. (2017). In contrast, SSW2019 exhibited a nearly neutral NAM in the troposphere, and is classified as a non-downward-influencing SSW (Rao et al., 2020).

For both SSW2018 and SSW2019, the later-initialized NUDGED and CONTROL experiments are compared (four days before the SSW2018 onset and six days after the SSW2019 onset), whereby their differences represent the stratospheric contribution to surface impacts. The internal variability is minimized by using 50 ensemble members for each model. The inter-model variability is also reduced by examining the multi-model ensemble mean (MME), comprising five of the models participating in the SNAPSI project (Table 1). While the SNAPSI project includes additional models, only five models provide the extrapolated subsurface data necessary for the analysis in the present study.

Table 1. SNAPSI models used in this study.

Institution	Model	Atmospheric resolution	Reference
CNR-ISAC	GLOBO	0.7° × 0.5°, top 0.15 hPa	Malguzzi et al. (2011)
ECMWF	IFS	TCo319, top 0.01 hPa	ECMWF documentation
KMA	GloSea6	N216, top 85 km	Walters et al. (2017)

https://doi.org/10.5194/egusphere-2026-2798
Preprint. Discussion started: 1 June 2026

Météo-France	CNRM-CM6-1	TL359, top 0.01 hPa	Voldoire et al. (2019)
SNU	GRIMs	T126, top 0.3 hPa	Koo et al. (2023)

2.2 Decomposition of tropospheric anomalies

Tropospheric responses of SSW are primarily examined with polar-cap-averaged geopotential height anomalies which are closely related with the NAM (Baldwin and Thompson, 2009). In particular, their differences between NUDGED and CONTROL experiments are investigated. The geopotential height differences between the two experiments are decomposed into contributions of temperature and surface pressure, following the method used in Mudryk and Kushner (2011) and Hong and Son (2025), as shown in Eq. (1).

$$\Delta Z \approx -\frac{R}{g}\int_{p_{s,C}}^{p}\frac{\Delta T}{p'}dp' + \frac{R}{g}T_{s,C}\frac{\Delta p_s}{p_{s,C}}, \quad (1)$$

where Z is the geopotential height, T the air temperature, p the pressure, p_s the surface pressure, $g = 9.81\ m\ s^{-2}$ the gravitational acceleration, $R = 287.05\ J\ kg^{-1}\ K^{-1}$ the gas constant for dry air. The subscript C denotes the CONTROL experiment, and the delta (Δ) denotes the difference between NUDGED and CONTROL experiments. The two terms in the r.h.s. represent the geopotential height differences related with differences in temperature and surface pressure, respectively. While the first term represents the change in thickness due to temperature below the given level, the second term accounts for the effect of surface pressure change.

2.3 Polar-cap averaged surface pressure budget

The temporal evolution of the polar-cap averaged surface pressure, averaged over the polar cap from 60°N to the pole, can be understood with the following equation.

$$\frac{\partial}{\partial t}\left(\int_{60°N}^{90°N}\bar{p_s}cos\varphi\ d\varphi\right) = \frac{1}{a}\int_{1000\ hPa}^{0\ hPa}(\tilde{\rho}\bar{v}cos\varphi)_{60°N},\ \ where\ \tilde{\rho} = dp, \quad (2)$$

where v is the meridional wind, φ the latitude, $a = 6.371 \times 10^6\ m$ the radius of earth, and an overbar represents the zonal mean. The pseudodensity $\tilde{\rho}$, which is defined as the vertical pressure difference, acts as mass. The r.h.s. represents the total mass flux across the Arctic Circle (60°N), which is the same as mass convergence over the polar cap, and explains the polar-cap averaged surface pressure change in Eq. (1).

2.4 Kuo-Eliassen equation

The Kuo-Eliassen (KE) equation (Kuo 1956), which is driven by combining the quasi-geostrophic (QG) momentum and thermodynamic equations under thermal wind balance, is utilized to diagnose the meridional circulation, or $\bar{v}$ in Eq. (2).

$$\nabla^2\bar{\psi} = \frac{R}{ap}\frac{\partial\bar{Q}}{\partial\varphi} - f\frac{\partial\bar{X}}{\partial p} - \frac{R}{a^2p}\frac{\partial}{\partial\varphi}\left[\frac{1}{\cos\varphi}\frac{\partial}{\partial\varphi}(\overline{v'T'}\cos\varphi)\right] + \frac{f}{a\cos^2\varphi}\frac{\partial^2}{\partial p\partial\varphi}(\overline{u'v'}\cos^2\varphi), \quad (3)$$

https://doi.org/10.5194/egusphere-2026-2798
Preprint. Discussion started: 1 June 2026

where $\bar{\psi} = \frac{2\pi a \cos\varphi}{g}\int_0^p \bar{v}\, dp$ is the mass stream function, Q the diabatic heating, f the Coriolis parameter, X the zonal drag, $\nabla^2 = f^2 \frac{g}{2\pi a \cos\varphi}\frac{\partial^2}{\partial p^2} + \frac{R}{ap}\frac{g}{2\pi a}\frac{\partial}{\partial\varphi}\left(\frac{\Gamma}{a\cos\varphi}\frac{\partial}{\partial\varphi}\right)$ the Laplacian operator, $\Gamma = \frac{R\bar{T}}{c_p p} - \frac{\partial\bar{T}}{\partial p}$ the static stability, and $c_p = 1{,}004\ J\ kg^{-1}\ K^{-1}$ the specific heat capacity. Since not all models provide both nudging and parameterized tendencies, diabatic heating and zonal drag are derived as residuals in the Eulerian-mean thermodynamic and momentum equations, respectively. Consequently, these terms incorporate the combined effects of nudging and parameterization.

The KE equation describes the relationship between the ageostrophic circulation (the mass streamfunction on the l. h. s. of Eq. (3)) and the QG forcings (terms on the r. h. s. of Eq. (3)). Thus, it accounts for how the ageostrophic circulation develops to restore the thermal wind balance when disrupted by QG forcings. The resulting circulation can be diagnosed by inverting the equation. For the surface boundary condition, we apply the following equation from Haynes and Shepherd (1989).

$$\frac{RT_s}{a^2 p}\frac{\partial}{\partial\varphi}\left(\frac{1}{\cos\varphi}\frac{\partial\bar{\psi}}{\partial\varphi}\right) - \frac{f^2}{\cos\varphi}\frac{\partial\bar{\psi}}{\partial p} = f\frac{\partial\bar{X}}{\partial p} - \frac{f}{a\cos^2\varphi}\frac{\partial^2}{\partial p\partial\varphi}\left(\overline{u'v'}\cos^2\varphi\right), \quad (4)$$

where T_s is the surface air temperature. The meridional circulation difference is then decomposed into the contributions from diabatic heating, drag, eddy heat flux, and eddy momentum flux, as shown in Eq. (5).

$$\Delta\bar{\psi} = \Delta\bar{\psi}_{\bar{Q}} + \Delta\bar{\psi}_{\bar{X}} + \Delta\bar{\psi}_{\overline{v'T'}} + \Delta\bar{\psi}_{\overline{u'v'}}, \quad (5)$$

3 Results

3.1 SSW2018 versus SSW2019

The tropospheric anomaly during SSW2018 exhibited a positive polar-cap geopotential height anomaly (Fig. 1a), consistent with a negative phase of NAM. This shift was accompanied by a negative North Atlantic Oscillation (NAO), triggering significant surface extremes, such as European cold air outbreaks and record-breaking rainfall in the Iberian Peninsula (Ayarzagüena et al., 2018; Lü et al., 2020; Dai et al., 2025). The tropospheric anomaly peaked at the surface when scaled by the daily standard deviation at each pressure level. This is more evident in polar-cap pressure anomaly (Fig. 1c), representing surface amplification of SSW. However, a persistent positive anomaly did not follow the SSW2019 (Fig. 1b). Although the positive anomaly was present in late January and early February, the one-moth-averaged tropospheric anomaly remains near neutral. The differing surface impacts are also evident in the polar-cap surface pressure anomalies (cf. Figs. 1c,d). These results indicate that SSWs differ in surface impacts, i.e., downward-influencing SSW2018 event and non-downward-influencing SSW2019 event.

https://doi.org/10.5194/egusphere-2026-2798
Preprint. Discussion started: 1 June 2026

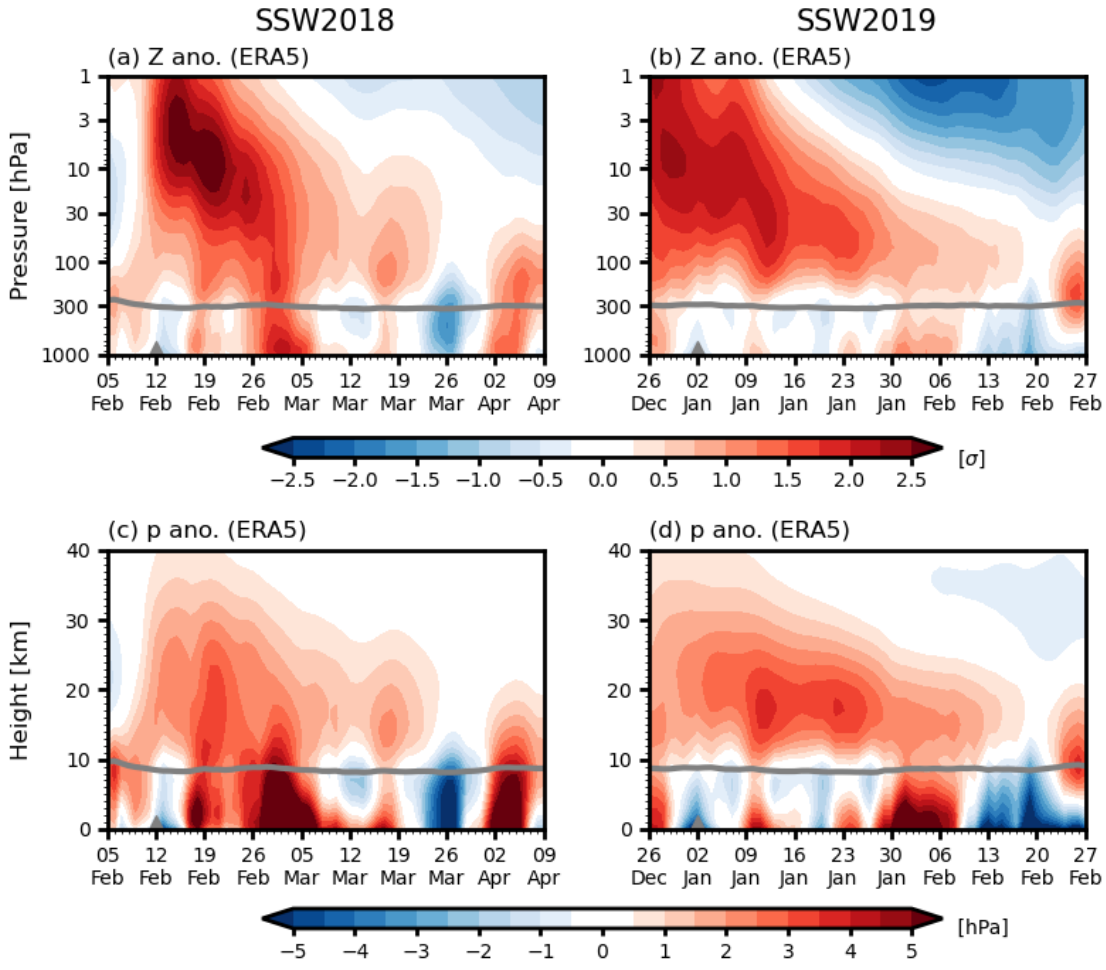

Figure 1. Polar cap (60-90°N) averaged geopotential height anomalies during the (a) SSW2018 and (b) SSW2019. (c, d) Same as (a, b) but for the pressure anomalies in the height coordinate. The geopotential height anomalies are scaled by the daily standard deviation at each pressure level and air pressure is calculated from geopotential height in the pressure coordinate by using cubic spline interpolation. The gray triangles indicate the onset date of SSW. The horizontal thick gray line indicates the tropopause pressure or height.

Figure 2 illustrates the observed and simulated stratospheric winds. The FREE experiments (blue lines) well capture the observed evolution of polar vortex during SSWs (black lines), as models are initialized right before or after the SSW onset. However, the recovery of the polar vortex varies across models. For example, GLOBO (dotted blue line in Fig. 2a) exhibits a rapid recovery during SSW2018, while GRIMs (solid blue line) exhibits a slow recovery. This inter-model spread complicates the interpretation of the stratosphere's role, as surface impacts inherently reflect these varying stratospheres. In contrast, the NUDGED (green lines) and CONTROL (red lines) experiments follow their reference states with minimal inter-model spread. By definition, while the stratospheric differences between the two experiments represent the anomalies specific to each SSW, those in the troposphere indicate the forced response to SSW. Despite identical zonal-mean SSW forcing, tropospheric

https://doi.org/10.5194/egusphere-2026-2798
Preprint. Discussion started: 1 June 2026

responses slightly differ across models due to different model resolution, physical parameterizations, and other factors, as shown later.

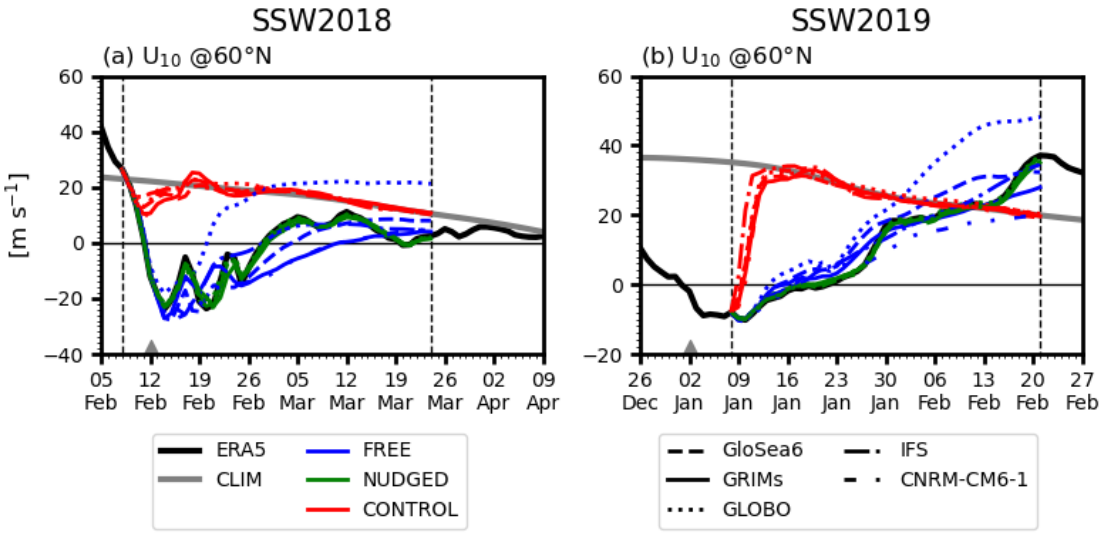

Figure 2. Time evolution of the ensemble-mean zonal-mean zonal wind at 60°N and 10 hPa for each model experiment during the (a) SSW2018 and (b) SSW2019. Models are distinguished by line styles (see legend in the bottom right). The gray triangles indicate the onset date of SSW. The solid black and gray lines represent the ERA5 and its climatology, respectively. Vertical dashed lines denote the starting and ending dates of the SNAPSI experiments analysed in this study.

3.2 Downward influence of SSW nudging

The standardized polar-cap geopotential height anomalies, averaged across all models, are examined to investigate the SSW-induced circulation changes (Fig. 3). During the SSW2018, the NUDGED experiments exhibit significant positive anomalies in both the stratosphere and troposphere (Fig. 3a). The tropospheric anomalies persist for about three weeks, from 15 February to 8 March, with amplitudes exceeding those in the lower stratosphere. This pattern resembles the surface amplification of SSW in the observations (see Fig. 1a), although the detailed temporal evolutions differ. In contrast, the CONTROL experiments simulate much weaker anomalies in the troposphere compared to the NUDGED experiments. Therefore, the differences between the two experiments follow the NUDGED experiments (Fig. 3e). When examining each model, all show positive anomalies in the troposphere, while CNRM-CM6-1 exhibits more pronounced anomalies compared to others (Fig. S1): this result is consistent with Garfinkel et al. (2025), who found that the CNRM-CM6-1 hindcasts suffer from overly strong coupling as compared to reanalysis data (see their Fig. 4).

https://doi.org/10.5194/egusphere-2026-2798
Preprint. Discussion started: 1 June 2026

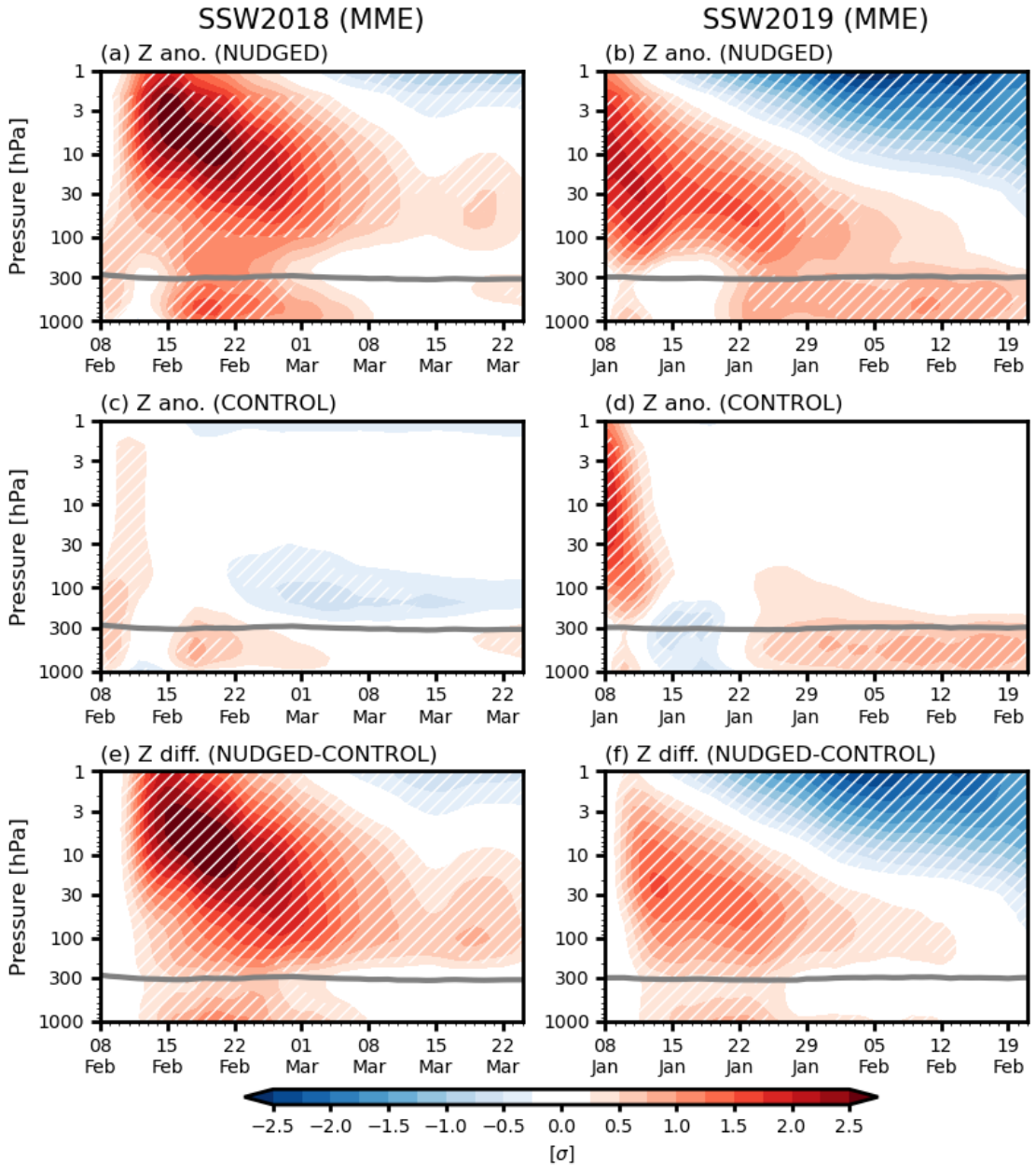

Figure 3. Same as Figs. 1a,b but for the multi-model ensemble-mean (MME) standardized geopotential height anomalies for the (a, b) NUDGED, (c, d) CONTROL experiments, and (e, f) their differences. The values with a consistent sign across all models are hatched. The horizontal thick gray line indicates the tropopause pressure.

Unlike the SSW2018, the SSW2019 was not accompanied by long-lasting tropospheric anomalies in the observations (see Fig. 1b). However, the NUDGED experiments simulate persistent positive anomalies in the troposphere from 20 January to

https://doi.org/10.5194/egusphere-2026-2798
Preprint. Discussion started: 1 June 2026

the end of simulation (Fig. 3b). These tropospheric anomalies are largely due to tropospheric processes, rather than stratospheric ones, as similar anomalies appear in the CONTROL experiments (Fig. 3d). However, the differences between the two experiments, i.e. downward influences of SSW, are evident in the first three weeks (Fig. 3f). This result suggests that, although the SSW2019 is classified as a non-downward-influencing event, the SSW still alters the tropospheric anomalies. Despite the SSW-induced anomalies in both SSW2018 and SSW2019 (Figs. 3e,f), the absence of SSW-related signal in the observations (Fig. 1b) is likely due to tropospheric processes which suppress these effects. This downward influence is present in all individual models (Fig. S2), highlighting the robustness of the results across the different models. Knight et al. (2021), who conducted nudging experiments for both SSW2018 and SSW2019 using the Met Office operational seasonal prediction system, also reported the same results.

The downward influence of nudged SSW is further examined for each model in Fig. 4. The geopotential height differences at 1000 hPa are averaged over about ten days, starting one week after initialization, when prominent differences are found in Figs. 3e,f. While ERA5 (black dashed line in Fig. 4) exhibits a stronger value (0.15) during SSW2018 compared to a near-neutral value (0.00) during SSW2019, all models show comparable values for both SSWs. Furthermore, all models overestimate the near-surface geopotential height differences with non-negligible inter-model spread. This suggests that SNAPSI nudging experiments overrepresent the stratosphere-troposphere coupling (Lee et al., 2025). This issue is discussed in a later section.

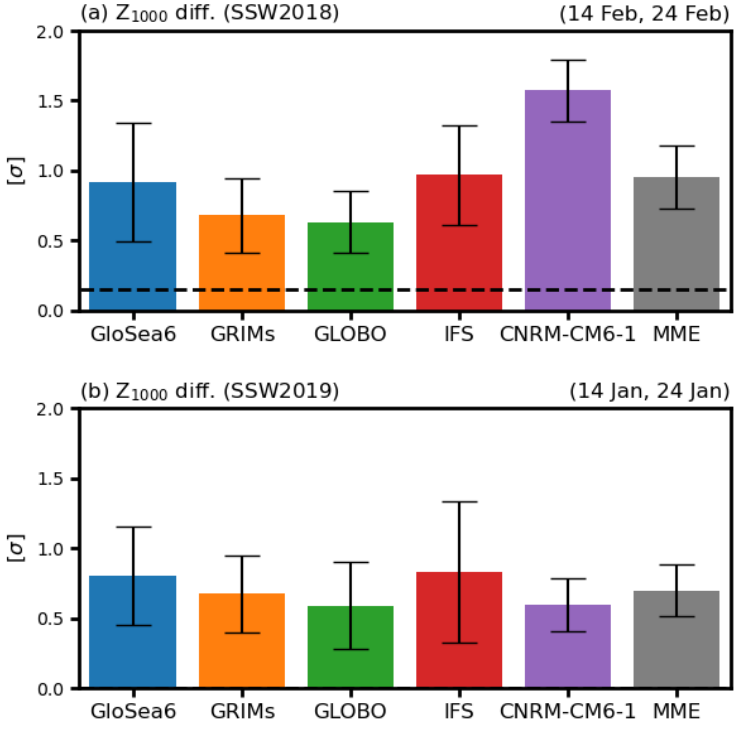

https://doi.org/10.5194/egusphere-2026-2798
Preprint. Discussion started: 1 June 2026

Figure 4. Bar plots of differences (NUDGED − CONTROL) in standardized polar-cap-averaged geopotential height at the surface (1000 hPa) averaged over approximately ten days, starting one week after initialization of the (a) SSW2018 and (b) SSW2019 experiments. Averaging periods are indicated in the upper right corner of each panel. Whiskers denote one standard deviation across the ensemble members. The horizontal black line indicates the ERA5 value.

These results suggest that both SSWs drive negative NAM. The observed tropospheric anomalies, differing between the SSW2018 and SSW2019 (Fig. 1), are likely due to internal variability in the troposphere which overwhelms SSW-forced anomalies. Below, the mechanisms through which SSW drives tropospheric anomalies are explored. All analyses are conducted with multi-model ensemble (MME) values.

3.3 How does SSW nudging alter tropospheric anomalies?

The geopotential height responses to SSW nudging (Figs. 3e,f) are first decomposed into contributions from temperature and surface pressure (Fig. 5; see Eq. (1)). Although the nonlinear component is neglected, the reconstructed geopotential height differences (Figs. 5a,b) are almost identical to those shown in Figs. 3e,f. The decomposition reveals that the temperature increase in the stratosphere by SSW nudging contributes to the geopotential height increase only in the stratosphere (Figs. 5c,d), whereas the tropospheric geopotential height increase, with maximum at the surface, is mainly attributed to surface pressure increase (Figs. 5e,f). It implies that SSWs alter the tropospheric anomalies through mass redistribution, instead of a time-lagged direct downward propagation of sudden warming. Note that while the pressure-related geopotential height component in Eq. (1) is independent of height, its vertical structure exhibits a maximum at the surface. This is due to the normalization by the standard deviation at each level, which is smallest at the surface.

The key factor that determines SSW-forced surface anomalies, more specifically positive geopotential height anomalies or negative NAM, is the surface pressure increase over the Arctic. This result is consistent with the composite analysis of SSWs in observations (see Fig. 1 of Hong and Son, 2025). It suggests that, even though the SSW is nudged in the model experiments, its downward influence may follow the mechanism consistent with observations.

https://doi.org/10.5194/egusphere-2026-2798
Preprint. Discussion started: 1 June 2026

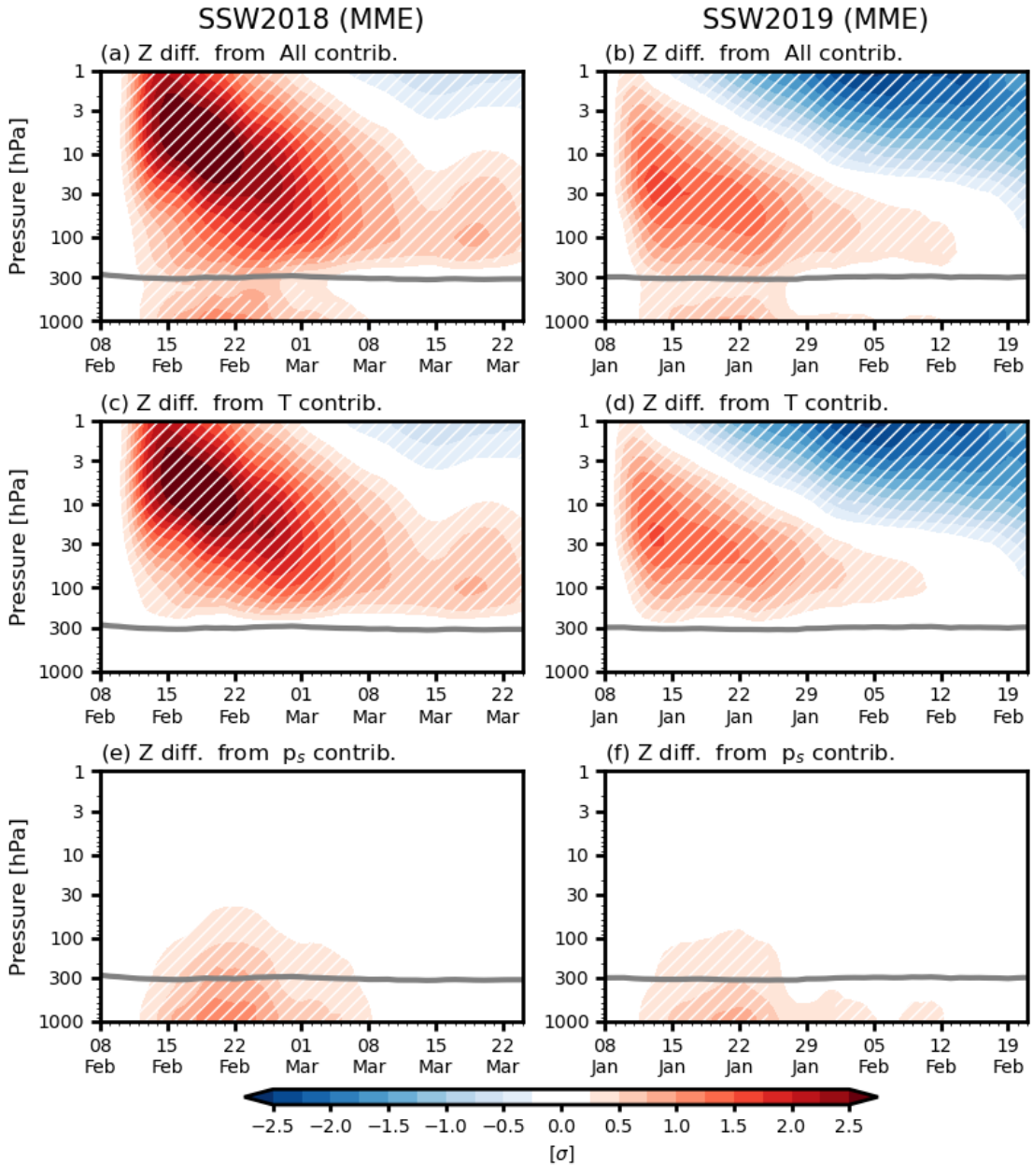

Figure 5. (a, b) Same as Figs. 3e,f but for the MME differences in standardized geopotential height, reconstructed from Eq. (1). Note that top panels are almost identical to Figs. 3e,f, indicating the validity of Eq. (1). The contributions of (c, d) temperature and (e, f) surface pressure differences to the total differences (a, b) are presented in bottom two rows.

The Arctic surface pressure rises immediately after SSW nudging and remains significant for about four weeks (Figs. 6a,b). To examine its temporal evolution, a polar-cap averaged surface pressure budget is analyzed using Eq. (2). Although the budget

https://doi.org/10.5194/egusphere-2026-2798
Preprint. Discussion started: 1 June 2026

(gray lines in Figs. 6c,d) occasionally overestimates or underestimates the surface pressure change (black lines in Figs. 6c,d) possibly due to the coarse vertical resolution of the post-processed model output, it qualitatively captures the surface pressure change. It clearly shows that poleward mass transport across the Arctic circle (r.h.s. of Eq. (2)), which leads to the polar-cap averaged surface pressure increase, is significantly positive during the first two weeks of the model integration. The mass convergence within 10 days after SSW nudging plays a key role in driving the initial SSW downward influence.

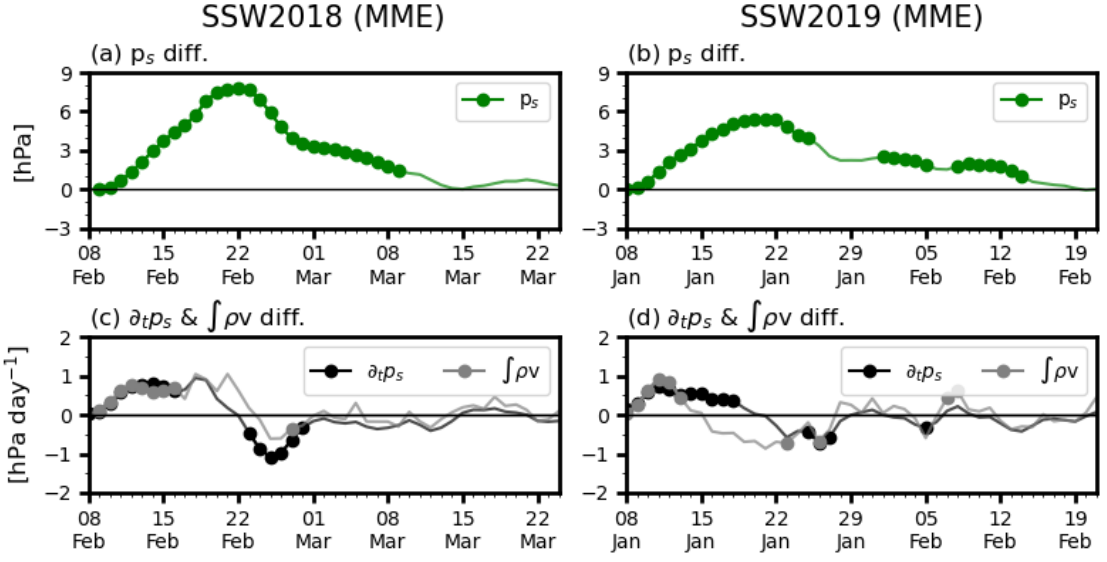

Figure 6. (top) Time evolution of MME differences in the polar-cap-averaged surface pressure (green) during the (a) SSW2018 and (b) SSW2019. (c, d) Same as (a, b) but for the tendency (black) and the budget derived from Eq. (2) (gray). Closed circles indicate values with a consistent sign across all models.

The mass convergence over the Arctic, or poleward mass transport across the Arctic Circle in the atmosphere, is further analyzed in terms of the poleward mass flux across 60°N at each vertical level (Figs. 7a,b). SSW nudging drives a significant poleward mass flux in the middle stratosphere, followed by equatorward mass flux near the surface at the beginning. This stratospheric mass flux, likely a direct response to the SSW nudging, is stronger than the near-surface return flow, resulting in an Arctic surface pressure increase. Subsequently, a poleward mass flux develops near the tropopause (gray lines) with a slightly weaker equatorward mass flux near the surface, contributing to the increase or maintenance of Arctic surface pressure. This dipolar structure, comprising a poleward mass flux near the tropopause and an equatorward mass flux near the surface, is consistent with the composite analysis of SSWs in the observations (see Fig. 3 of Hong and Son, 2025), although the equatorward mass flux appears earlier than the observations.

https://doi.org/10.5194/egusphere-2026-2798
Preprint. Discussion started: 1 June 2026

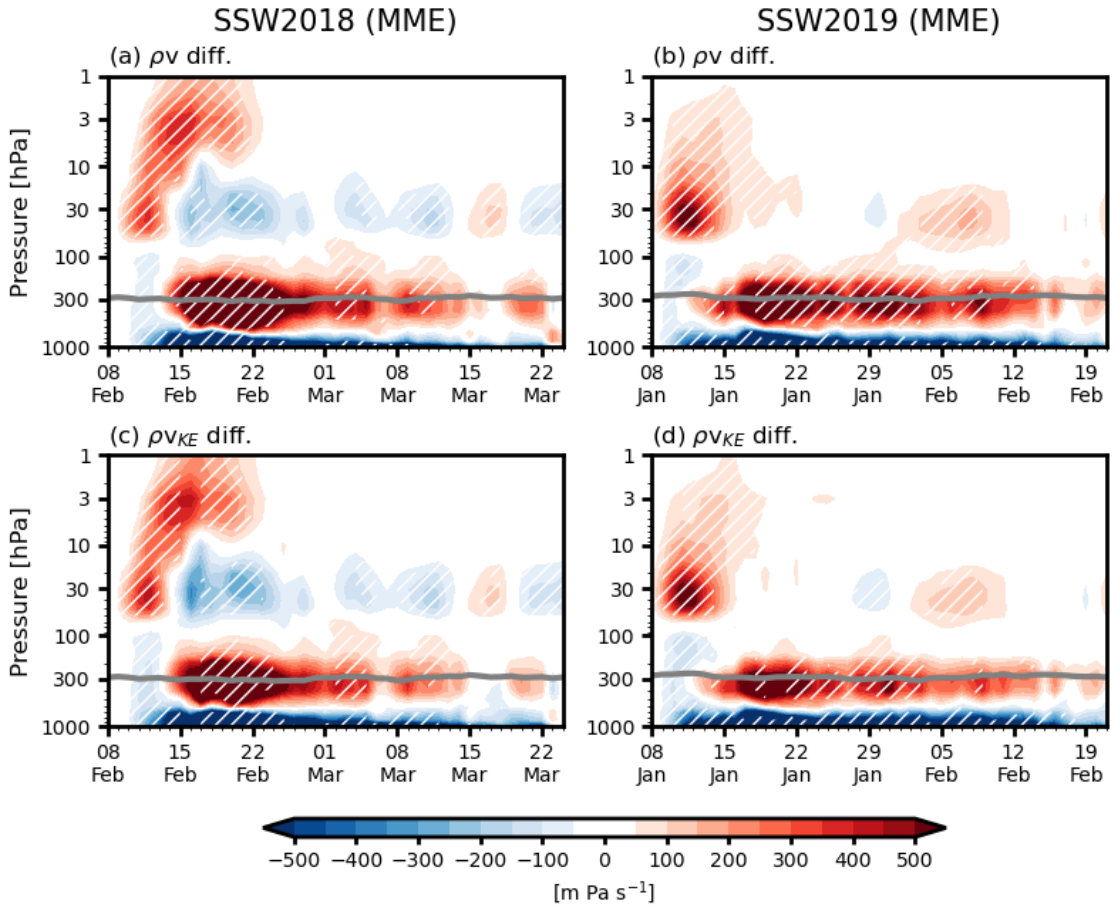

Figure 7. (a, b) Vertical profile of MME differences in poleward mass flux at 60°N between the NUDGED and CONTROL experiments. The values with a consistent sign across all models are hatched. (c, d) Same as (a, b) but for the poleward mass flux differences derived from the Eq. (3). Horizontal thick gray line indicates the tropopause pressure.

The Kuo-Eliassen equation (KE eq.; Eq. (3)) is employed to investigate the mass flux during SSW nudging. The KE eq. is derived by combining the QG momentum and thermodynamic equations under thermal wind balance. It diagnoses the ageostrophic circulation which restores thermal wind balance when disrupted by the QG forcings. Owing to the linearity of the equation, the diagnosed ageostrophic circulation can be decomposed into contributions from individual processes (Eq. (5)).

The mass flux differences between the NUDGED and CONTROL experiments reconstructed from the KE eq. are illustrated in Figs. 7c,d. They quantitatively capture the main features of the mass flux differences in Figs. 7a,b. This allows us to examine individual processes that determine mean meridional circulation and poleward mass flux (Fig. 8). As anticipated, the zonal drag accounts for the initial dipolar mass flux structures between the stratosphere and the troposphere (Figs. 8a,b). It also contributes to persistent dipolar mass fluxes between the tropopause and the surface after one week of initialization. A similar dipolar structure also appears due to eddy momentum flux, but with much stronger magnitude near the tropopause than the zonal drag (Figs. 8c,d). While the eddy heat flux also plays a role in initial and subsequent dipolar structures (Figs. 8e,f), its

https://doi.org/10.5194/egusphere-2026-2798
Preprint. Discussion started: 1 June 2026

magnitude is considerably smaller than those of the zonal drag and eddy momentum flux. The contribution of diabatic heating is negligible (Figs. 8g,h).

The zonal drag contributes to the initial poleward mass flux in the stratosphere (Figs. 8a,b). This poleward mass flux is concentrated above approximately 70 hPa and lasts for about one week. It alters the tropospheric anomalies without time lag. While an equatorward mass flux forms below approximately 100 hPa with a maximum at the surface as a part of the return flow, it is insufficient to offset the surface pressure increase driven by the poleward mass flux in the stratosphere. These initial responses are mostly due to the SSW nudging: note that the SNAPSI nudging begins at 90 hPa and reaches full strength at 50 hPa (Hitchcock et al., 2022). As the zonal drag, shown in Figs. 8a,b, encompasses zonal wind nudging and parameterized drag such as surface damping, and turbulent dissipations, their relative roles are further examined in Fig. 9. When the direct effects of nudging are separated from the parameterized processes, initial responses within a week are dominated by the nudging (Figs. 9c,d). The parameterized processes become active more than five days into the model integrations when tropospheric circulation changes become sufficiently strong (Figs. 9e,f). Note that Figs. 9a,b slightly differ from Figs. 8a,b, as GloSea6 is discarded due to data availability.

About two weeks later, an equatorward mass flux develops in the middle stratosphere as the polar vortex recovers (Figs. 9c,d), with that near the surface being maintained (Figs. 9e,f). Their net effects are stronger than poleward mass flux near the tropopause (Figs. 7c,d), leading to the reduction in Arctic surface pressure after two weeks of model integration (Figs 6c,d). As a result, the contribution of zonal wind drag to Arctic surface pressure switches from an increase to decrease.

https://doi.org/10.5194/egusphere-2026-2798
Preprint. Discussion started: 1 June 2026

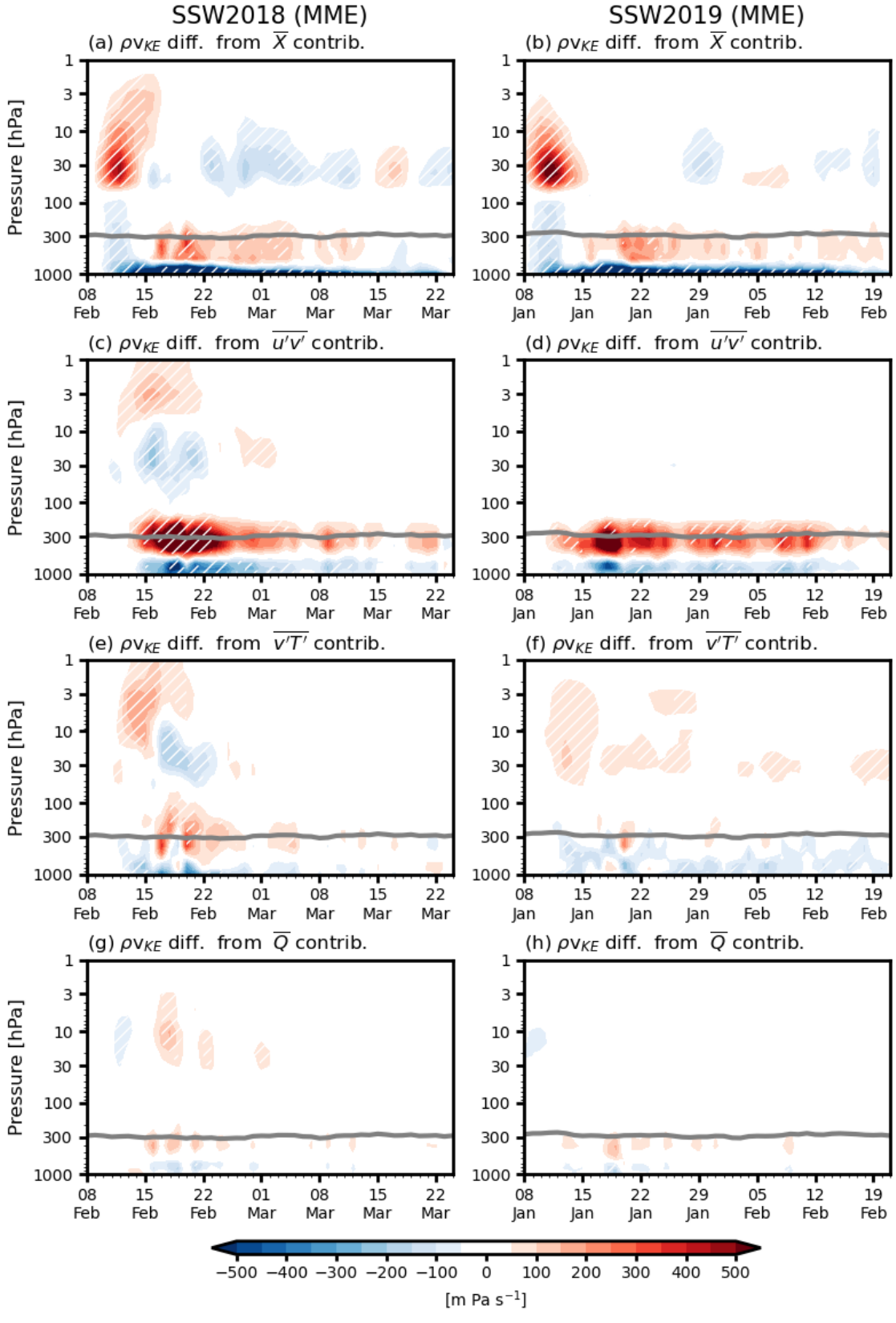

https://doi.org/10.5194/egusphere-2026-2798
Preprint. Discussion started: 1 June 2026

Figure 8. Same as Figs. 7c,d but for the poleward mass flux derived from the Eq. (3): (a, b) zonal drag, (c, d) eddy momentum flux, (e, f) eddy heat flux, and (g, h) diabatic heating differences. The zonal drag and diabatic heating are calculated as the residual in the Eulerian-averaged momentum and thermodynamic equations, respectively. Note that sum of each contribution is identical to Figs. 7c, d.

The eddy momentum flux plays a major role in driving the poleward mass flux near the tropopause during SSW nudging (Figs. 8c,d), accounting for the Arctic surface pressure increase approximately five days after model integration in both cases. The momentum flux also contributes to relatively deep equatorward mass flux in the lower troposphere compared to the shallow return flow induced by zonal drag (compare with Figs. 8a,b). However, as the equatorward mass flux in the lower troposphere is weaker than poleward mass flux near the tropopause, the eddy momentum flux leads to an increase in Arctic surface pressure. This result is consistent with previous studies highlighting the importance of eddy-mean flow interaction (e.g., Hitchcock and Simpson, 2016; White et al., 2020). The delayed response of momentum flux with respect to the zonal drag further suggests that eddy-mean flow interaction is organized by SSW-related mean flow changes. It is noteworthy from Fig. 8c that a dipolar mass flux also appears in the middle stratosphere, but only during SSW2018, revealing differences in upper-stratospheric eddy activity between events.

SSW nudging also modifies eddy heat fluxes (Figs. 8e,f). However, their contributions are generally weaker and shorter-lasting than those from the zonal drag and eddy momentum flux, making a limited contribution to the Arctic surface pressure change. The diabatic heating makes no meaningful contribution to the mass flux differences during both SSW events (Figs. 8g,h). This also holds for the individual contributions from temperature nudging and parameterized heating (Fig. S3). The negligible role of diabatic heating is also reported in the observational study by Hong and Son (2025).

https://doi.org/10.5194/egusphere-2026-2798
Preprint. Discussion started: 1 June 2026

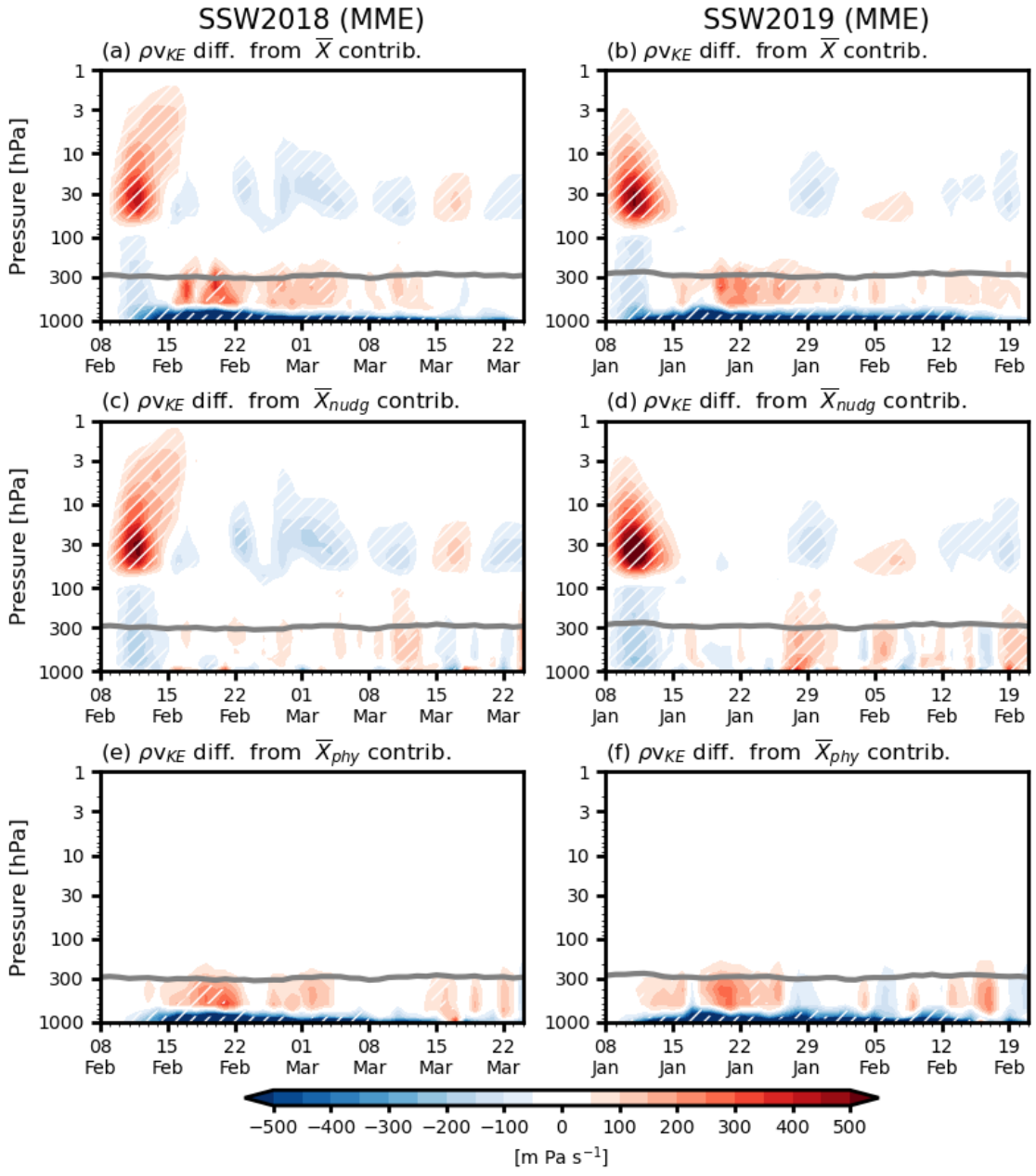

Figure 9. (a, b) Same as Figs. 8a,b, but for four models except GloSea6 due to data availability, and contributions of (c,d) the zonal-mean zonal wind nudging and (e, f) parameterized zonal wind tendency. Note that the sum of the middle and bottom panels is identical to the top panel.

https://doi.org/10.5194/egusphere-2026-2798
Preprint. Discussion started: 1 June 2026

3.4 Meridional circulation change by SSW nudging

The mass flux changes induced by QG forcings are further investigated through an analysis of the mean meridional circulation response to SSW nudging, using $\Delta\bar{\psi}$ in Eq. (5). Figure 10 illustrates the zonal-wind nudging tendency and the associated mass flux changes (vectors in Fig. 10) in the initial period from days +0 to +6, when SSW nudging plays a critical role in Figs. 8a,b (see also Figs. 9c,d). By definition, the significant easterly forcing by SSW nudging (polar vortex weakening) appears above approximately 70 hPa in both SSW cases. This easterly forcing diminishes the vertical wind shear, thereby disrupting the thermal wind balance. To restore this balance, an ageostrophic circulation develops, comprising poleward flow (Coriolis acceleration) above 70 hPa and equatorward flow (Coriolis deceleration) below. This ageostrophic circulation is responsible for a poleward mass flux in the middle stratosphere and an equatorward mass flux below 70 hPa across the Arctic Circle (Figs. 9c,d).

While the zonal wind nudging induces the strong meridional circulation (Figs. 10; see also Figs. 9c,d), the meridional circulation driven by temperature nudging is not only considerably weaker but also opposite in direction (Figs. S4). The sudden warming induced by temperature nudging drives a divergent flow in the polar stratosphere, thereby suppressing surface pressure increase. A weaker impact of temperature nudging is consistent with previous studies: White et al. (2020, 2022) reported that while temperature-forced SSWs exhibit a delayed tropospheric response, momentum-forced SSWs produce a fast and strong poleward mass transport in the stratosphere.

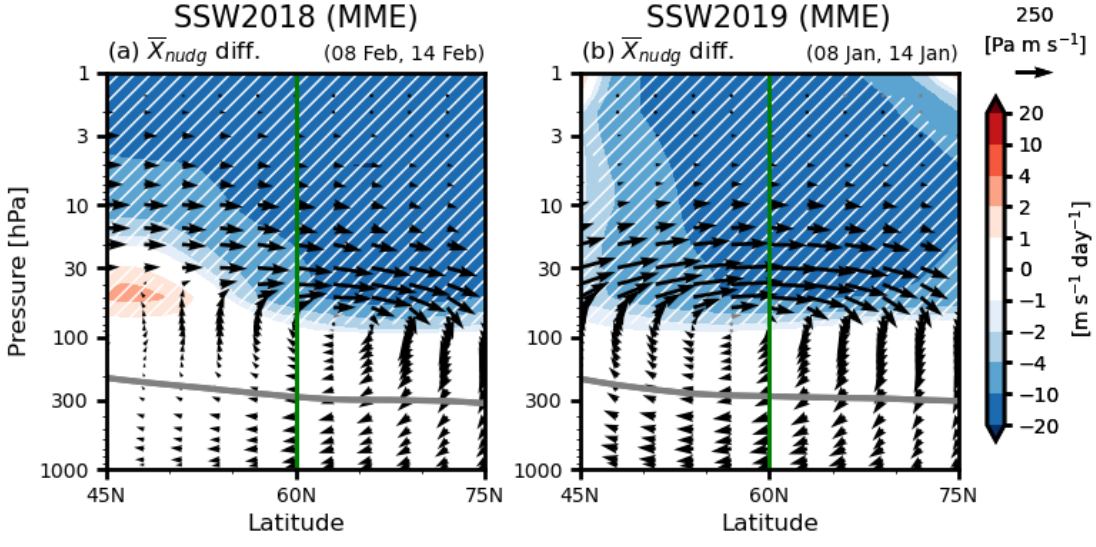

Figure 10. Latitude-pressure cross sections of MME differences in zonal wind nudging tendency (shading) and the associated mass flux (arrows) averaged over day +0 to +6 after the initialization of the (a) SSW2018 and (b) SSW2019 experiments. The gray and green lines indicate the tropopause pressure and 60°N latitude (Arctic Circle), respectively. The values with a consistent sign across all models are hatched or indicated with black arrows.

https://doi.org/10.5194/egusphere-2026-2798
Preprint. Discussion started: 1 June 2026

330 Approximately four days after the model initialization, a negative eddy heat flux develops in the high-latitude upper stratosphere from days +4 to +10 (Figs. 11a,b). This eddy heat flux change is dominated by planetary-scale disturbances with zonal wavenumber equal to and less than three, which is consistent with prohibited or weakened vertical propagation of planetary-scale waves in the stratosphere under SSW. Here, it should be noted that, unlike observations where SSWs are driven by anomalous upward-propagating waves, the SSWs in the present study are prescribed by the nudging. As the nudging is 335 applied exclusively to the zonal-mean state and not to the eddy, the resulting eddy heat flux does not have a one-to-one correspondence with the anomalous wave activity during SSWs in the observations. Instead, the heat flux change represents the effects of the SSW-related stratospheric mean state on wave propagation, which causes the negative eddy heat flux difference (blue shading in Figs. 11a,b).

This negative eddy heat flux results in warming to the south and cooling to the north, inducing upward (adiabatic cooling) 340 and downward (adiabatic warming) motions, respectively, in the polar stratosphere. To maintain continuity, a weak clockwise circulation develops in the high-latitude upper stratosphere, driving a weak poleward mass flux in the region (poleward vectors across 60°N in Figs. 11a,b; see also Figs. 8e,f). A comparison between the two SSW cases reveals that the SSW2018 exhibits a stronger eddy heat flux response than the SSW2019, leading to a stronger poleward mass flux in the upper stratosphere (cf. Figs. 8e,f).

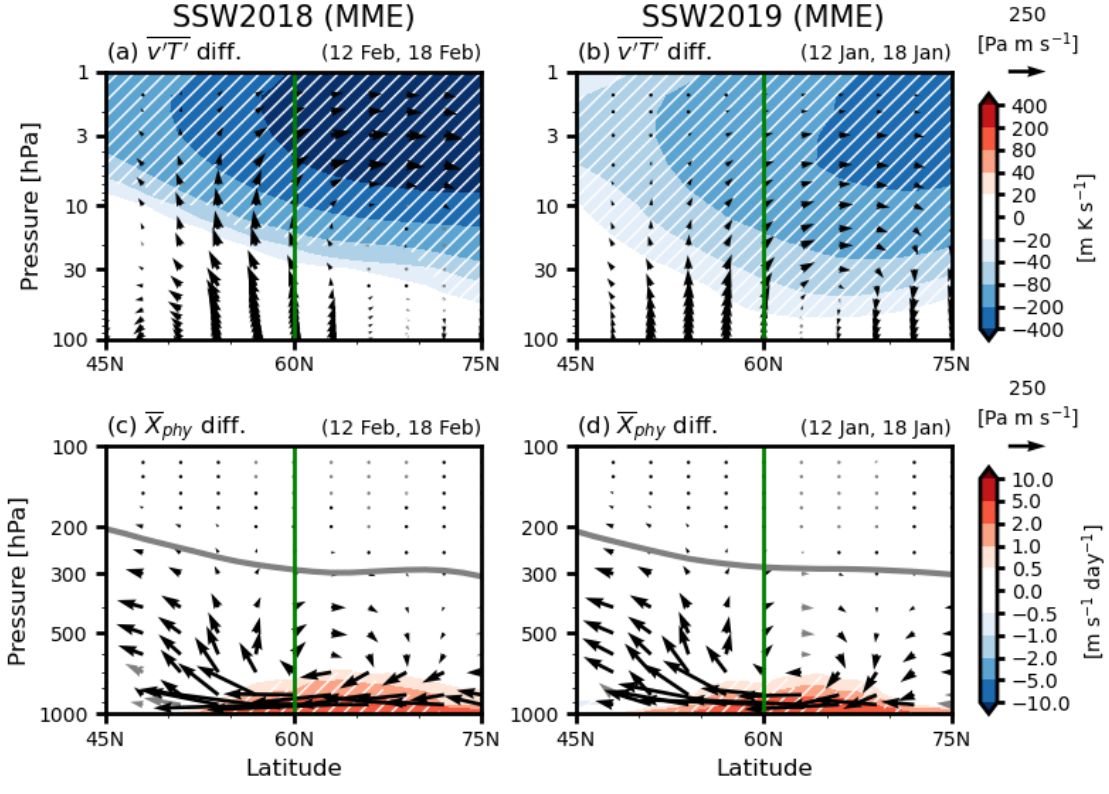

345

https://doi.org/10.5194/egusphere-2026-2798
Preprint. Discussion started: 1 June 2026

Figure 11. Same as Fig. 10 but for the (a, b) eddy heat flux and (c, d) parameterized zonal wind tendency averaged over day +4 to +10 after the initialization. Note that the vertical range for top and bottom panels are different.

The parameterized zonal wind tendency, which incorporates boundary layer damping, turbulent diffusion, and gravity wave drag, exhibits a westerly forcing near the surface in most of the integration period. It is confined to the high-latitude surface, representing weakened damping (Figs. 11c,d). The weakened damping results from near-surface northerly wind due to anomalous high pressure in the Arctic which decelerates the zonal wind near the surface through Coriolis deceleration (easterly forcing). This drives anomalous westerly forcing near the surface (by weakened damping). Similar to the zonal wind nudging tendency shown in Fig. 10, this response weakens the vertical wind shear in the lower troposphere. To restore the thermal wind balance, a strong equatorward flow (Coriolis deceleration) develops near 60°N in the lower troposphere, while a weak poleward flow develops in the upper troposphere (see vectors in Figs. 11c,d). This near-surface mass flux then acts to weaken the Arctic surface pressure increase, indicating a negative feedback from surface drag, consistent with previous studies (e.g., Hitchcock and Simpson, 2016; Hong and Son, 2025).

The above results suggest that poleward mass flux in the stratosphere within the first 10 days develops as a direct response to SSW nudging, followed by two indirect responses. The reduction of vertically propagating waves induced by easterly winds associated with nudged SSW leads to poleward mass transport in the stratosphere. An equatorward mass flux develops near the surface as a negative feedback that offsets the increase in Arctic surface pressure.

After one week of initialization, a persistent negative eddy momentum flux develops with peaks around 50–55°N in the upper troposphere and lower stratosphere from days +6 to +16 (Figs. 12a,b). The easterly forcing, driven by eddy momentum flux divergence north of the minimum peak, decelerates the zonal wind and weakens the high-latitude vertical wind shear. To restore the vertical wind shear, a clockwise circulation emerges. The upper branch of this circulation induces poleward mass transport (upper-level vectors in Figs. 12a,b; see also Figs. 8c,d), serving as the primary contributor to the increase in Arctic surface pressure approximately one week after initialization. An equatorward mass flux also develops in the lower level due to continuity (lower-level vectors in Figs. 12a,b). However, its intensity is weaker than the one induced by surface drag (Figs. 12c,d; see also Figs. 11c,d). As this return flow by eddy momentum flux and surface drag only partially offsets the poleward mass flux near the tropopause, the net result is a slight increase in Arctic surface pressure (see Figs 6c,d).

This negative eddy momentum flux and associated mass flux persist for more than a month until the end of model integration, which is consistent with previous studies (e.g., Hitchcock and Simpson, 2016; White et al., 2020). The eddy momentum flux response in the model develops with a time lag, due to initial cancelation between the NUDGED and CONTROL experiments when waves (or eddy momentum flux) are not strongly influenced by SSW nudging. White et al. (2020) and Hong and Son (2025) suggested that mean-state changes during SSW tend to induce waves propagating more poleward, consistent with the negative eddy momentum flux, through wave guidance. These waves are in both synoptic and planetary scales (Fig. S5), as reported by Hong and Son (2025).

https://doi.org/10.5194/egusphere-2026-2798
Preprint. Discussion started: 1 June 2026

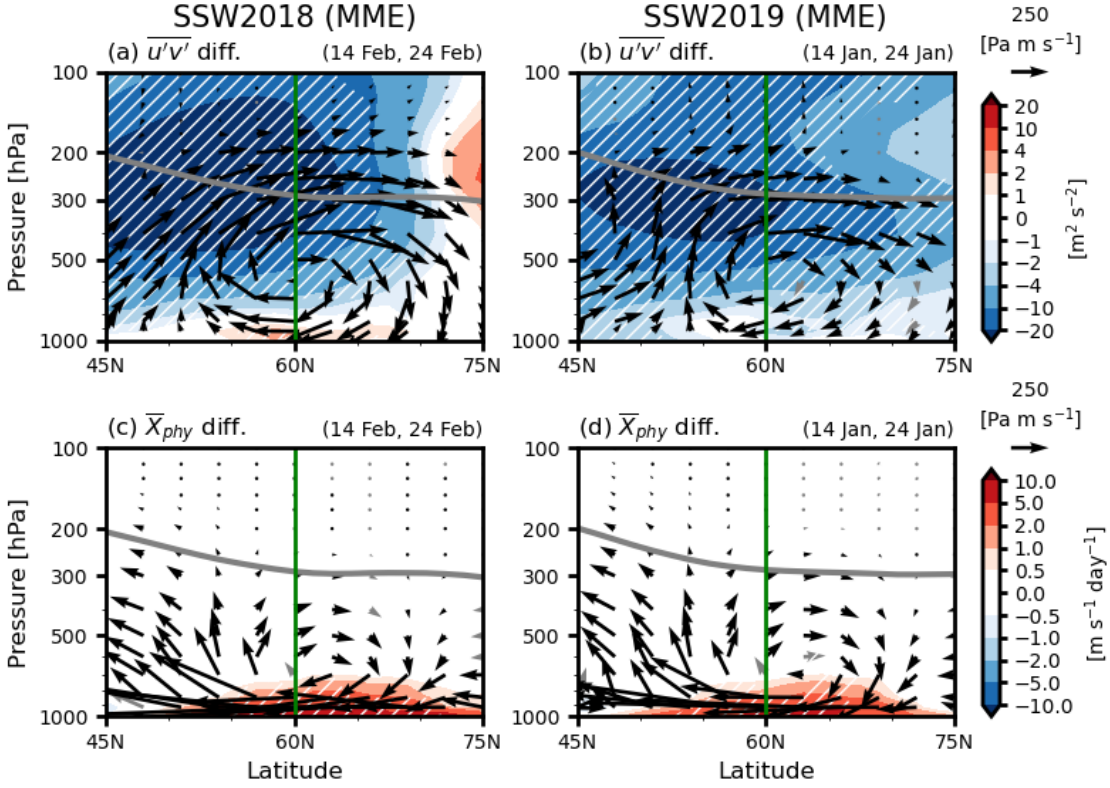

Figure 12. Same as Fig. 10 but for the (a, b) eddy momentum flux and (c, d) parameterized zonal wind tendency averaged over day +6 to +16 after the initialization. Note that the averaging periods are longer than those in Figs. 10 and 11.

The relationship between the persistence of eddy momentum flux and the resulting surface response is further illustrated in Fig. 13. Figure 13 presents scatter plots of polar-cap-averaged geopotential height at 1000 hPa against eddy momentum flux divergence at 60°N and 300 hPa, averaged over the same periods as in Fig. 4 and Fig. 12. During both SSW cases, all models exhibit statistically significant positive correlations, underscoring the critical role of eddy momentum flux in the persistent downward influence of SSW. Furthermore, all models show stronger momentum flux divergence compared to ERA5 for both cases. This discrepancy is particularly pronounced for SSW2018, where ERA5 exhibits a negative value; this suggests that the overestimation of the NAM during SSW2018 (Fig. 4a) may stem from an exaggerated eddy momentum flux in nudging experiments. For SSW2019, although the eddy momentum flux divergence in ERA5 is comparable to those in models, the observed surface anomaly in ERA5 is much smaller. However, this still remains within the ensemble spread, indicating the importance of internal variability.

Consequently, while the downward influence is initiated by SSW nudging, it is maintained through eddy-mean flow interaction. Although a detailed analysis of eddy momentum flux divergence is beyond the scope of the present study due to

https://doi.org/10.5194/egusphere-2026-2798
Preprint. Discussion started: 1 June 2026

its stochastic nature, these results suggest that nudged SSWs also influence the troposphere through eddy-mean flow interaction in the upper troposphere and lower stratosphere.

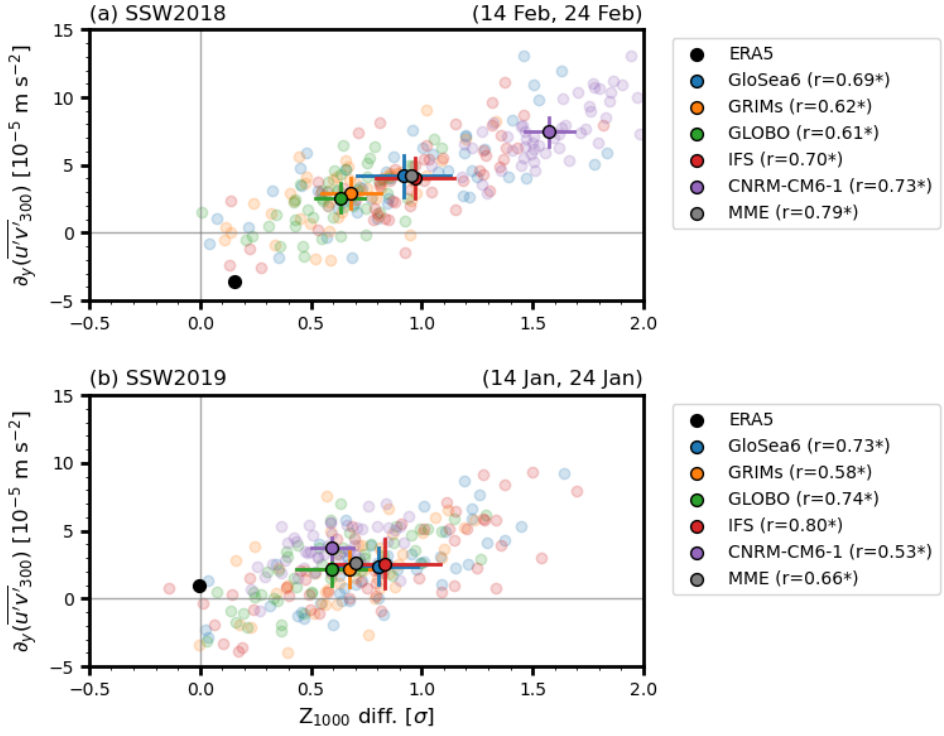

Figure 13. Scatter plots of differences (NUDGED − CONTROL) in standardized polar-cap-averaged geopotential height at the surface (1000 hPa) against eddy momentum flux divergence near the tropopause (300 hPa) at 60°N, averaged over day +6 to +16 after the initialization of the (a) SSW2018 and (b) SSW2019 experiments. While dark-colored dots with bars indicate the ensemble mean and the ensemble spread measured by one standard deviation, light-colored dots indicate each ensemble member. The correlation coefficients (r) for each model and MME are indicated at the legends. Statistically significant values at the 95% confidence level, based on the two-tailed Student's t-test, are denoted with an asterisk. The black dot indicates the ERA5 value.

4 Summary and Discussion

The present study investigates the forced responses of the tropospheric circulation to SSW by analyzing SSW nudging experiments. While the observed surface anomalies following the February 2018 SSW (SSW2018) and January 2019 SSW (SSW2019) differ, the forced surface responses to these two events, which are quantified by differencing SSW nudging experiments (NUDGED) and climatological nudging experiments (CONTROL), exhibit similar negative NAM patterns. The SSW-induced tropospheric anomalies mainly result from the Arctic surface pressure increase, which is primarily driven by the sequential poleward mass flux. Initially the zonal wind nudging (forced polar vortex weakening) directly drives the poleward mass flux in the stratosphere. The eddy heat flux change, representing modulation of vertical wave propagation by the nudged background wind in the stratosphere, plays a secondary role. Subsequently, the eddy momentum flux sustains the poleward mass flux near the tropopause, appearing roughly one week later. This poleward mass flux is slightly stronger than the

https://doi.org/10.5194/egusphere-2026-2798
Preprint. Discussion started: 1 June 2026

equatorward mass flux near the surface, resulting from parameterized zonal wind drag. These processes are nearly identical for both the 2018 and 2019 SSW cases, showing only minor differences in detail.

These results suggest that the differing surface responses to SSWs in the observations do not originate from the stratosphere. Using tropical forcing experiments, Knight et al. (2021) quantified the responses to tropical forcing during SSW events. While the tropical conditions during SSW2018, a strong Madden-Julian Oscillation (MJO), induced a negative NAM in February, the conditions during SSW2019, a weak El Niño, hindered the negative NAM during the first half of January. This pattern is also evident in both the NUDGED and CONTROL experiments of the present study (see Figs. 3b,d). Consequently, Knight et al. (2025) highlight the role of internal variability in the absence of downward SSW influence, which is smoothed out by ensemble averaging in the present study. Although mid-latitude internal variability, such as the Ural ridge (Zhang et al., 2024), is beyond our current scope, further studies are required to clarify its specific role.

The simulated surface impacts of SSWs and underlying dynamical processes resemble those in observations (Hong and Son, 2025). Specifically, the persistent poleward mass flux near the tropopause and equatorward mass flux near the surface, driven by eddy momentum flux and zonal drag (or parameterized processes), consistently developed. A key difference, however, is mass flux in the upper stratosphere near the SSW onset. While the observed SSWs exhibit a transition from equatorward to poleward mass flux in the upper stratosphere near the onset (Fig. 3b of Hong and Son, 2025), the poleward mass flux is more prominent during the initial SSW nudging in the present study. This difference stems from the triggering mechanism of SSW. In observations, SSWs are often triggered by anomalous upward-propagating waves, and anomalous upward wave propagation switches to downward due to the easterly mean state in the stratosphere following the SSW. Accordingly, Hong and Son (2025) reported that while eddy heat flux induces an equatorward mass flux in the stratosphere prior to SSW onset, the resulting equatorward mass flux is significantly weakened after the SSW onset (Figs. 6a,d in Hong and Son, 2025).

In the present study, however, the SSW, temperature difference between the NUDGED and CONTROL experiments, is triggered by artificial nudging. Furthermore, since the nudging is applied only to the zonal-mean component of the stratosphere and not to the eddy component, both the NUDGED and CONTROL experiments have nearly identical eddy activities during the initial period. Consequently, the eddy heat flux differences do not show the anomalous upward-propagating waves or the resulting equatorward mass fluxes in the upper stratosphere (see Figs. 11a,b). Instead, downward or weakened upward-propagating waves and subsequent poleward mass fluxes are presented. As temperature nudging replaces the role of eddy heat flux in triggering SSWs, it similarly induces a divergent flow in the upper stratosphere albeit with a much weaker amplitude compared to the observations (Fig. S4).

Multi-model analyses reveal a substantial inter-model spread in surface anomalies. For instance, surface anomalies in the CNRM-CM6-1 are about two times larger than those in GLOBO during SSW2018 (Fig. 4a). This inter-model spread can be attributed to model resolution, physical parameterizations, and coupling processes. Specifically, tropospheric responses can be sensitive to surface drag which determines the equatorward return flow near the surface after SSWs. In this regard, idealized model experiments where surface drag is systematically varied could provide insights to addressing this issue.

https://doi.org/10.5194/egusphere-2026-2798
Preprint. Discussion started: 1 June 2026

Data availability

The SNAPSI datasets used in the present study are archived by CEDA https://catalogue.ceda.ac.uk/uuid/0a5a1ce22fb047749e040879efa8e9b5/. ERA5 reanalysis datasets are available through https://cds.climate.copernicus.eu/datasets/reanalysis-era5-pressure-levels.

Author contributions

D.-C.H. and S.-W.S. designed the study and wrote the first draft of the manuscript. D.-C.H. performed the analysis. All authors discussed the results and edited the manuscript.

Competing interests

At least one of the (co-)authors is a member of the editorial board of *Weather and Climate Dynamics*. The authors have no other competing interests to declare.

Disclaimer

Publisher's note: Copernicus Publications remains neutral with regard to jurisdictional claims made in the text, published maps, institutional affiliations, or any other geographical representation in this paper. While Copernicus Publications makes every effort to include appropriate place names, the final responsibility lies with the authors. Views expressed in the text are those of the authors and do not necessarily reflect the views of the publisher.

Acknowledgements

The GRIMs model was performed with the computational support from the KISTI National Supercomputing Center with supercomputing resources including technical support (KSC-2022-CRE-0249). This work used JASMIN, the UK's collaborative data analysis environment (https://www.jasmin.ac.uk, last access: 13 May 2026) (Lawrence et al., 2013).

Financial support

This work was supported by the National Research Foundation of Korea (NRF) Grant funded by the Korea government (MSIT) (2023R1A2C3005607). B.A. acknowledges support from the grant PID2024-158151NB-I00 funded by MICIU/AEI/10.13039/501100011033 and ERDF/EU. C.I.G. is supported by the ISF–NSFC joint research program (Israel Science Foundation grant no. 3065/23). P.H. acknowledges support from the National Science Foundation, grant 2340133.

https://doi.org/10.5194/egusphere-2026-2798
Preprint. Discussion started: 1 June 2026

Review statement

References

Ayarzagüena, B., Barriopedro, D., Garrido-Perez, J. M., Abalos, M., De La Cámara, A., García-Herrera, R., Ordóñez, C., and others: Stratospheric connection to the abrupt end of the 2016/2017 Iberian drought, Geophys. Res. Lett., 45, 12639–12646, https://doi.org/10.1029/2018GL079802, 2018.

Ayarzagüena, B., Butler, A. H., Hitchcock, P., Garfinkel, C. I., Lawrence, Z. D., Ning, W., Stockdale, T., and others: The role of the stratospheric state in upward wave flux prior to Sudden Stratospheric Warmings: a SNAPSI analysis, Weather Clim. Dynam., 7, 411–437, https://doi.org/10.5194/wcd-7-411-2026, 2026.

Baldwin, M. P., and Dunkerton, T. J.: Stratospheric harbingers of anomalous weather regimes, Science, 294, 581–584, https://doi.org/10.1126/science.1063315, 2001.

Baldwin, M. P., and Thompson, D. W.: A critical comparison of stratosphere–troposphere coupling indices, Q. J. R. Meteorolog. Soc., 135, 1661-1672, https://doi.org/10.1002/qj.479, 2009.

Baldwin, M. P., Ayarzagüena, B., Birner, T., Butchart, N., Butler, A. H., Charlton-Perez, A. J., Pedatella, N. M., and others: Sudden stratospheric warmings, Rev. Geophys., 59, e2020RG000708, https://doi.org/10.1029/2020RG000708, 2021.

Butler, A. H., Sjoberg, J. P., Seidel, D. J., and Rosenlof, K. H.: A sudden stratospheric warming compendium, Earth Syst. Sci. Data, 9, 63–76, https://doi.org/10.5194/essd-9-63-2017, 2017.

Butler, A. H., Charlton-Perez, A., Domeisen, D. I. V., Garfinkel, C. I., Gerber, E. P., Hitchcock, P., Karpechko, A. Y., Maycock, A. C., Son, S.-W., and Thompson, C.: Subseasonal predictability and the stratosphere, *Sub-seasonal to Seasonal Prediction (Second Edition)*, Elsevier, 355–397, https://doi.org/10.1016/B978-0-443-31538-1.00006-3, 2026.

Dai, Y., Hitchcock, P., Butler, A. H., Garfinkel, C. I., and Seviour, W. J. M.: Assessing stratospheric contributions to subseasonal predictions of precipitation after the 2018 sudden stratospheric warming from the Stratospheric Nudging And Predictable Surface Impacts (SNAPSI) project, Weather Clim. Dynam., 6, 841–862, https://doi.org/10.5194/wcd-6-841-2025, 2025.

Domeisen, D. I. and Butler, A. H.: Stratospheric drivers of extreme events at the Earth's surface, Commun. Earth Environ., 1, 59, https://doi.org/10.1038/s43247-020-00060-z, 2020.

Garfinkel, C. I., Lawrence, Z. D., Butler, A. H., Dunn-Sigouin, E., Erner, I., Karpechko, A. Y., Koren, G., and others: A process-based evaluation of biases in extratropical stratosphere–troposphere coupling in subseasonal forecast systems. Weather and Climate Dynamics, 6, 171-195, https://doi.org/10.5194/wcd-6-171-2025, 2025.

Haynes, P. H. and Shepherd, T. G.: The importance of surface pressure changes in the response of the atmosphere to zonally-symmetric thermal and mechanical forcing, Q. J. R. Meteorolog. Soc., 115, 1181–1208, https://doi.org/10.1002/qj.49711549002, 1989.

https://doi.org/10.5194/egusphere-2026-2798
Preprint. Discussion started: 1 June 2026

Hersbach, H., Bell, B., Berrisford, P., Hirahara, S., Horányi, A., Muñoz-Sabater, J., Thépaut, J. N., and others: The ERA5 global reanalysis, Q. J. R. Meteorolog. Soc., 146, 1999–2049, https://doi.org/10.1002/qj.3803, 2020.

Hitchcock, P., Shepherd, T. G. and Manney, G. L.: Statistical characterization of arctic polar-night jet oscillation events, J. Clim., 26, 2096-2116, https://doi.org/10.1175/JCLI-D-12-00202.1, 2013.

Hitchcock, P. and Simpson, I. R.: Quantifying eddy feedbacks and forcings in the tropospheric response to stratospheric sudden warmings, J. Atmos. Sci., 73, 3641–3657, https://doi.org/10.1175/JAS-D-16-0056.1, 2016.

Hitchcock, P., Butler, A., Charlton-Perez, A., Garfinkel, C. I., Stockdale, T., Anstey, J., Hendon, H., and others: Stratospheric Nudging And Predictable Surface Impacts (SNAPSI): a protocol for investigating the role of stratospheric polar vortex disturbances in subseasonal to seasonal forecasts, Geosci. Model Dev., 15, 5073–5092, https://doi.org/10.5194/gmd-15-5073-2022, 2022.

Hong, D.-C. and Son, S.-W.: Surface amplification of stratospheric sudden warming by poleward mass flux in the upper troposphere and lower stratosphere, J. Clim., 38, 5069–5082, https://doi.org/10.1175/JCLI-D-24-0597.1, 2025.

Huang, J., Hitchcock, P., Tian, W., and Sillin, J.: Stratospheric influence on the development of the 2018 late winter European cold air outbreak, J. Geophys. Res. Atmos., 127, e2021JD035877, https://doi.org/10.1029/2021JD035877, 2022.

Karpechko, A. Y., Hitchcock, P., Peters, D. H., and Schneidereit, A.: Predictability of downward propagation of major sudden stratospheric warmings, Q. J. R. Meteorolog. Soc., 143, 1459–1470, https://doi.org/10.1002/qj.3017, 2017.

Knight, J., Scaife, A., Bett, P. E., Collier, T., Dunstone, N., Gordon, M., Walker, B., and others: Predictability of European Winters 2017/2018 and 2018/2019: Contrasting influences from the Tropics and stratosphere, Atmos. Sci. Lett., 22, e1009, https://doi.org/10.1002/asl.1009, 2021.

Kodera, K., Mukougawa, H., Maury, P., Ueda, M., and Claud, C.: Absorbing and reflecting sudden stratospheric warming events and their relationship with tropospheric circulation, J. Geophys. Res. Atmos., 121, 80–94, https://doi.org/10.1002/2015JD023359, 2016.

Koo, M.-S., Song, K., Kim, J.-E. E., Son, S.-W., Chang, E.-C., Jeong, J.-H., Hong, S.-Y., and others: The global/regional integrated model system (GRIMs): an update and seasonal evaluation, Asia-Pac. J. Atmos. Sci., 59, 113–132, https://doi.org/10.1007/s13143-022-00297-y, 2023.

Kuo, H. L.: Forced and free meridional circulations in the atmosphere, J. Atmos. Sci., 13, 561–568, https://doi.org/10.1175/1520-0469(1956)013<0561:FAFMCI>2.0.CO;2, 1956.

Lee, R. W., Charlton-Perez, A. J., and Lee, S. H.: Stratospheric impacts on weather regimes following the 2018 and 2019 sudden stratospheric warmings, Geophys. Res. Lett., 52, e2025GL115668, https://doi.org/10.1029/2025GL115668, 2025.

Lü, Z., Li, F., Orsolini, Y. J., Gao, Y., and He, S.: Understanding of European cold extremes, sudden stratospheric warming, and Siberian snow accumulation in the winter of 2017/18, J. Clim., 33, 527–545, https://doi.org/10.1175/JCLI-D-18-0861.1, 2020.

https://doi.org/10.5194/egusphere-2026-2798
Preprint. Discussion started: 1 June 2026

Malguzzi, P., Buzzi, A., and Drofa, O.: The meteorological global model GLOBO at the ISAC-CNR of Italy assessment of 1.5 yr of experimental use for medium-range weather forecasts, Weather Forecast., 26, 1045–1055, https://doi.org/10.1175/WAF-D-11-00027.1, 2011.

Meehl, G. A., Richter, J. H., Teng, H., Capotondi, A., Cobb, K., Doblas-Reyes, F., Xie, S. P., and others: Initialized Earth System prediction from subseasonal to decadal timescales, Nat. Rev. Earth Environ., 2, 340–357, https://doi.org/10.1038/s43017-021-00155-x, 2021.

Mudryk, L. R. and Kushner, P. J.: A method to diagnose sources of annular mode time scales, J. Geophys. Res. Atmos., 116, D14, https://doi.org/10.1029/2010JD015291, 201R1.

Rao, J., Garfinkel, C. I., and White, I. P.: Predicting the downward and surface influence of the February 2018 and January 2019 sudden stratospheric warming events in subseasonal to seasonal (S2S) models, J. Geophys. Res. Atmos., 125, e2019JD031919, https://doi.org/10.1029/2019JD031919, 2020.

Scherhag, R.: Die explosionsartigen Stratosparenerwarmungen des Spatwinters 1952, Ber. Dtsch. Wetterdienstes US Zone, 38, 51, 1952.

Seviour, W. J. M., Finkel, J., Rupp, P., Mudhar, R., Butler, A. H., Garfinkel, C. I., Hitchcock, P., Ayarzagüena, B., Hong, D.-C., Hyun, Y.-K., Kim, H., Lim, E.-P., De Maeseneire, D., Messori, G., Koren, G., Sigmond, M., Simpson, I. R., and Son, S.-W.: Forecast-based attribution of the role of stratospheric variability in weather extremes, EGUsphere [preprint], https://doi.org/10.5194/egusphere-2026-230, 2026.

Voldoire, A., Saint-Martin, D., Sénési, S., Decharme, B., Alias, A., Chevallier, M., Waldman, R., and others: Evaluation of CMIP6 deck experiments with CNRM-CM6-1, J. Adv. Model. Earth Syst., 11, 2177–2213, https://doi.org/10.1029/2019MS001683, 2019.

Walters, D., Boutle, I., Brooks, M., Melvin, T., Stratton, R., Vosper, S., Xavier, P., and others: The Met Office unified model global atmosphere 6.0/6.1 and JULES global land 6.0/6.1 configurations, Geosci. Model Dev., 10, 1487–1520, https://doi.org/10.5194/gmd-10-1487-2017, 2017.

White, I. P., Garfinkel, C. I., Gerber, E. P., Jucker, M., Hitchcock, P., and Rao, J.: The generic nature of the tropospheric response to sudden stratospheric warmings, J. Clim., 33, 5589–5610, https://doi.org/10.1175/JCLI-D-19-0697.1, 2020.

White, I. P., Garfinkel, C. I., and Hitchcock, P.: On the tropospheric response to transient stratospheric momentum torques, J. Atmos. Sci., 79, 2041–2058, https://doi.org/10.1175/JAS-D-21-0237.1, 2022.

Zhang, C., Zhang, J., Maycock, A. C., and Tian, W.: Distinct tropospheric anomalies during sudden stratospheric warming events accompanied by strong and weak Ural Ridge. npj Climate and Atmospheric Science, 7, 280, https://doi.org/10.1038/s41612-024-00826-8,2024